Mid-21st century projections in temperature extremes in the southern Colorado Rocky Mountains from regional climate models

Imtiaz Rangwala · Joseph Barsugli · Karen Cozzetto · Jason Neff · James Prairie

Abstract This study analyzes mid-21st century projections of daily surface air minimum (T_{min}) and maximum (T_{max}) temperatures, by season and elevation, over the southern range of the Colorado Rocky Mountains. The projections are from four regional climate models (RCMs) that are part of the North American Regional Climate Change Assessment Program (NARCCAP). All four RCMs project 2°C or higher increases in T_{min} and T_{max} for all seasons. However, there are much greater (>3°C) increases in T_{max} during summer at higher elevations and in T_{min} during winter at lower elevations. T_{max} increases during summer are associated with drying conditions. The models simulate large reductions in latent heat fluxes and increases in sensible heat fluxes that are, in part, caused by decreases in precipitation and soil moisture. T_{min} increases during winter are found to be associated with decreases in surface snow cover, and increases in soil moisture and atmospheric water vapor. The increased moistening of the soil and atmosphere facilitates a greater diurnal retention of the daytime solar energy in the land surface and amplifies the longwave heating of the land surface at night. We hypothesize that the presence of significant surface moisture fluxes can modify the effects of snow-albedo feedback and results in greater wintertime warming at night than during the day.

I. Rangwala · J. Barsugli
Physical Sciences Division, NOAA Earth System Research
Laboratory, Boulder, CO, USA

Present Address:
I. Rangwala (✉)
Department of Marine and Coastal Sciences, Rutgers University,
71 Dudley Road, New Brunswick, NJ, USA
e-mail: rangwala@marine.rutgers.edu

K. Cozzetto · J. Neff
Geological Sciences Department and Environmental Studies
Program, University of Colorado, Boulder, CO, USA

J. Prairie
Bureau of Reclamation, University of Colorado,
Boulder, CO, USA

1 Introduction

Land and water resource managers in the western United States are starting to incorporate climate change into their planning process. In 2009, the Department of the Interior issued a secretarial order that requires consideration of climate change in planning activities (DOI 2009). The United States Forest Service has proposed an updated forest planning rule (USFS 2011) that also mandates that climate change be considered. Some examples of planning studies that are incorporating climate change in the Southern Colorado Rockies include climate change management plans being developed by the San Juan Public Lands Center (Kelly Palmer, pers. comm.), climate change vulnerability studies that are in progress for the Grand Mesa Uncompahgre Gunnison National Forest (Howe et al. 2011), and the West-Wide Climate Risk Assessment (USBR 2010) and the Colorado River Basin Water Supply and Demand Study (USBR 2009) being undertaken by the

United States Bureau of Reclamation. These studies rely largely on statistically downscaled climate projections to produce regional scale (<50 km) climate projections to inform their management plans for future climate change. Regional climate models (RCMs), nested in coupled atmosphere–ocean general circulation models (GCMs), are becoming more widely available to provide these regional climate projections (e.g., Giorgi et al. 2001; Moberg and Jones 2004; Liang et al. 2008). RCMs are found to provide a better skill in representing the present climate relative to GCMs, and are likely to capture non-linear physical processes in downscaling the GCM projections (Murphy 1999; Liang et al. 2008). RCMs also render a substantial improvement in representing the climate of mountainous regions (e.g. Salzmann et al. 2007).

Despite a better representation of the regional-scale climate processes, RCMs can still have significant biases in reproducing the present climate (e.g., Giorgi et al. 2001; Rummukainen et al. 2001; Vidale et al. 2003). These biases can systematically propagate into future projections at regional scales and their impacts on projected trends may also have a regional dependency (Liang et al. 2008). Seasonally, RCMs are found to be more skillful during winter as compared to summer (Murphy 1999; Vidale et al. 2003). Physical parameterization of various sub-grid scale processes in the RCM can strongly influence RCM's biases and skill (e.g., Murphy 1999; Hagemann et al. 2001; Rummukainen et al. 2001; Vidale et al. 2003). This can lead to different RCMs giving significantly different climate projections even when forced by identical lateral boundary conditions (Kjellström and Giorgi 2010). The systematic errors associated with the RCM formulation would need to be reduced to further improve RCM skills (Giorgi et al. 2001; Moberg and Jones 2004). Despite these uncertainties, the motivation of this paper is to provide a better understanding of the mechanisms that lead to climate change in the RCMs as well as the similarities and differences across models that can help us assess the robustness of the findings from the RCMs.

The Colorado Rocky Mountains have experienced a rapid warming trend since the mid-1990s (Ray et al. 2008; Rangwala and Miller 2010; Clow 2010). For the San Juan Mountains, Rangwala and Miller (2010) found that T_{min} and T_{max} are warming at similar rates (1°C/decade), although seasonally there were greater increases in T_{min} during winter and in T_{max} during summer. They also found greater warming at higher elevations in summer and at lower elevations in winter. The large daytime extremes in the summer temperature since the mid-1990s have not been seen in the past instrumental record (Rangwala and Miller 2011). While the observed changes in this region have not been formally attributed to anthropogenic causes, RCMs do show similar trends in the future, motivating a detailed analysis of the processes leading to these changes. Bonfils et al. (2008) found that recent (1950–1999) increases in late winter/early spring T_{min} and T_{max} in the mountainous regions of western United States were too rapid to be explained by natural climate variability alone.

In this study, we examine mid-21st century climate projections from multiple RCMs, driven by different GCMs, for the southern range of the Colorado Rocky Mountains which include the San Juan Mountains and Four Corners Region. We examine changes in T_{min} and T_{max} for this region from four RCM simulations available through the North American Regional Climate Change Assessment Program (NARCCAP; http://www.narccap.ucar.edu; Mearns et al. 2009). The experimental design of NARCCAP RCMs restricts us to assess only the mid-century (2041–2070) projections. As compared to the daily mean temperature, there is very limited assessment of projected changes in T_{min} and T_{max} in the prevailing literature, including the examination of climate drivers causing changes in these variables. T_{min} and T_{max} are generally affected differently by different climatic processes, and they are, usually, more relevant for impacts assessment than the mean daily temperature. We evaluate seasonal and elevational dependency of the responses in these two variables. We also analyze changes in the surface energy fluxes and other related climate variables to diagnose probable mechanisms for future changes in T_{min} and T_{max}. We have worked with land and water managers during the course of this study and we hope that this information will be of an importance to the regional land and water managers for their climate change assessment work. More specifically, this work will provide, (1) characterization and understanding of biases in the RCMs for selected climate variables, (2) identification of physical processes and mechanisms for climate change in the study region which could, for example, inform climate and impacts monitoring as part of an adaptive management strategy in response to climate change, and (3) aid in the development of process-based climate narratives for the region even in the face of uncertainty in the projected climate.

The next section discusses the RCMs considered and their validation for our study region. Section 3 describes the seasonally projected changes in T_{min}, T_{max} and the surface energy fluxes. Section 4 discusses the possible causes for these projected changes and Sect. 5 provides concluding statements.

2 Methods

The RCM simulations from NARCCAP have an approximately 50 km spatial resolution and were downscaled from GCM simulations forced by the Intergovernmental Panel

on Climate Change (IPCC) SRES A2 emissions scenario, which describes a future with continued high rates of greenhouse gas emissions. Based on the availability of output climate variables at the NARCCAP data archive (Mearns et al. 2007), we considered four RCM + GCM combinations in this analysis—CRCM+CGCM3, HRM3+HADCM3, RCM3+CGCM3 and WRFG+CCSM [RCMs: CRCM, HRM3, RCM3, WRFG; GCMs: CGCM3, HAD-CM3, CCSM]. Table 1 provides a description of these models. This selection covers a range of RCMs and the driving GCMs. The RCM+GCM output is only available for two different periods: 1969–2000 and 2039–2070. For our analysis, we ignore the first 2 years of output from both time periods because we consider them as the model spin-up periods. Most climate change anomalies described here are computed as differences between the 2041–2070 and 1971–2000 time periods.

The climate variables analyzed include T_{min}, T_{max}, precipitation, total cloud fraction, surface specific humidity, soil moisture, surface reflectivity and the major fluxes that contribute to the surface energy budget—upwelling (ULR) and downwelling (DLR) longwave radiation, absorption of solar radiation at surface (ASR; difference of downwelling and upwelling solar radiation at surface), and the latent (LAT) and sensible (SEN) heat fluxes. A complete set of output of these surface energy flux components and other climate variables was only available for two RCMs—CRCM+CGCM3 and HRM3+HADCM3—at the time of this analysis. Therefore, only these two RCMs are used to infer physical mechanisms for the projected seasonal changes in T_{min} and T_{max}. Further, we employ changes in surface reflectivity, determined as the ratio of the incoming to outgoing solar radiation, as a proxy for estimating changes in snow cover.

Figure 1 describes the study region. The region includes the San Juan Mountains and the Four Corners region to the west and south of these mountains. The San Juan Mountains are the southern extent of the Rocky Mountains in Colorado. The RCMs' surface elevation for the region varies between 1,500 m (5,000 ft) and 3,350 m (11,000 ft). Although this RCM elevation range does not represent the actual orographic variation from about 1,500 m to over 4,200 m (14,000 ft), it is a marked improvement from the orography found in most GCMs where the highest elevation is generally less than 2,500 m (8,000 ft) for this region. Furthermore, the regional scale features of the terrain in these RCMs are much improved relative to the GCMs. For example, the San Juan Mountains are resolved as a separate range in the RCMs considered here.

Both the inherent bias in an RCM as well as the bias in the GCM boundary forcings could influence the RCM projections. We analyzed output from the RCM experiments forced with the historical climate boundary conditions from NCEP Reanalysis-2, to compute the inherent RCM biases in T_{min} and T_{max} for the contiguous United States that may arise from differences in model parameterizations among the RCMs. Constrained by the availability of data, all biases were computed for the 1981–1999 period and they were calculated relative to the Maurer et al. (2002) observed monthly gridded data which is available at 1/8th degree spatial resolution. Caution should be exercised in interpreting the Maurer data as "truth" for the mountainous regions because there are significant differences among observed gridded datasets for these regions (Daly et al. 2008). All datasets were converted (Maurer—spatial averaging; NARCCAP—tension spline interpolation) to a standard half-degree grid before estimating the biases. Figures 2a and 3a show the inherent RCMs biases in T_{min} and T_{max}, respectively, for winter (Dec–Feb) and summer (Jun–Aug). We present these biases for the contiguous United States, in part, to relate the biases in our study region with biases at larger scale.

Table 1 Description of RCMs and GCMs considered in this study. More detail on these models could be obtained at http://www.narccap.ucar.edu

Acronym	Model name	Climate modeling center
Regional climate models		
CRCM	Canadian regional climate model	Ouranos, Canada
HRM3	Hadley regional model, v.3	Hadley Centre for Climate Prediction & Research, UK
RCM3	Regional climate model, v.3	University of California at Santa Cruz, US
WRFG	Weather research and forecasting model, Grell scheme	Pacific Northwest National Lab, US
General circulation models		
CCSM	Community climate system model, v.3	National Center for Atmospheric Research, US
CGCM3	Coupled global climate model, v.3.1	Canadian Centre for Climate Modeling and Analysis
HADCM3	Hadley centre coupled model, v.3	Hadley Centre for Climate Prediction & Research, UK
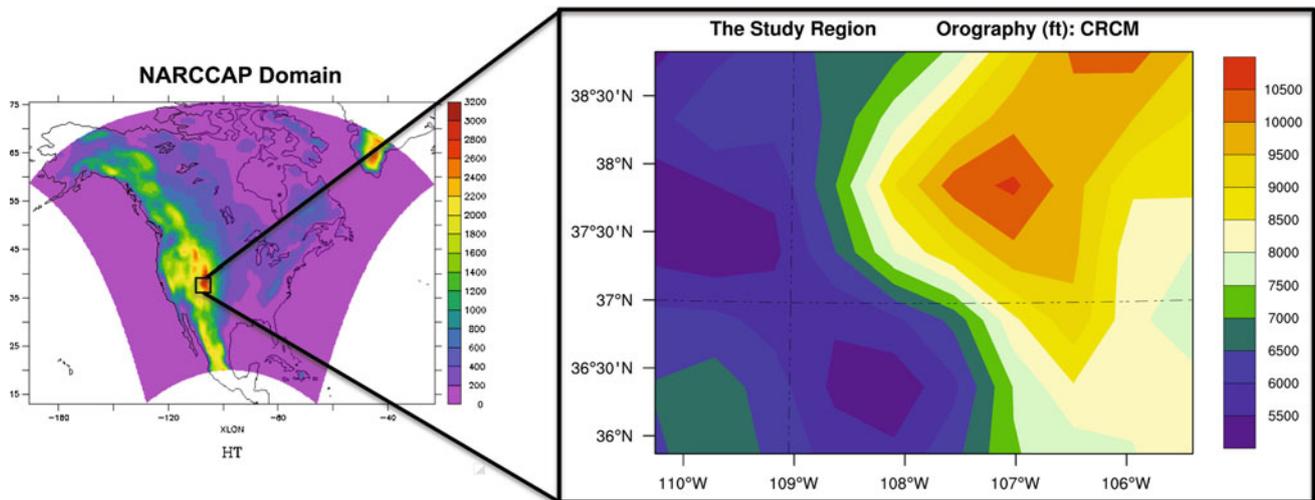
Fig. 1 The study region—the San Juan Mountains in the southwestern Colorado and the Four Corners region toward the west and south of them. The region's plot shows surface orography from one of the RCMs

Following exactly the same method as for the NCEP-forced runs, we also computed biases in T_{min} and T_{max} for the RCM experiments forced by different GCMs (Figs. 2b, 3b). We examine the influence of inherent biases in different RCMs, as found in Figs. 2a and 3a, on RCM projections when forced with different GCM boundary conditions. For T_{min}, we find that the RCM biases have a spatial coherence with the biases computed for RCMs forced with historical GCM boundary forcings for both winter and summer (Fig. 2). For example, CRCM has a cold bias in the western US which is also found in CRCM+CGCM3. On the other hand, HRM3 has a large warm bias in the western and central US which is reflected in HRM3+HADCM3. For T_{max}, the spatial coherence between RCM+NCEP and RCM+GCM biases are more apparent during summer (Fig. 3). For both T_{min} and T_{max}, we find that the inherent warm bias in an RCM is less pronounced in the associated RCM+GCM bias, whereas the inherent cold bias in an RCM is more pronounced in the associated RCM+GCM bias, particularly during winter. In evaluating the results for mid-21st century projections in T_{min} and T_{max} from these RCMs, we also consider the influence of historical biases that are reported here from RCM+NCEP and RCM+GCM experiments. Despite these biases, we find high correlation ($r = 0.5$–0.8) in the interannual variability between the reanalysis (NCEP) forced RCMs and the high resolution reanalysis data (NARR) for our study region (Table 2). The correlations tend to be higher in winter relative to summer.

Among the different RCMs examined here, CRCM is the only model which incorporates spectral nudging—where the spectral nudging is only carried out for the upper level horizontal winds. To evaluate any apparent influence of nudging on temperature biases in the RCMs, we examined historical biases in the winter and summer mean temperature in three GCM-driven RCMs and compared them with the biases from those three GCMs (Figure S1 in the Supplementary Material). The temperature biases in GCMs also show up in the RCMs to an extent which is similar for all cases, and therefore, we do not discern a significant influence of spectral nudging on the RCMs temperature biases.

3 Results

3.1 Projected changes in T_{min} and T_{max}

The changes in seasonal mean T_{min} and T_{max} between the two periods, 1971–2000 and 2041–2070, from the four RCM simulations are shown in Fig. 4. By mid-21st century, both T_{min} and T_{max} increase by more than 2°C in all seasons from all four simulations. Against the background of this general warming, two phenomena stand out: large increases in winter T_{min} and in summer T_{max}. T_{min} increases by 3–4°C in three of the four simulations. Summer, generally, has the next highest increase in T_{min} (~ 3°C). For T_{max}, all models show the largest increases during summer between 3and 4°C. Fall, in general, has the second highest increases in T_{max} (~ 3°C).

Winter has the largest spatial variability (1–3°C) in T_{min} increases for most of the simulations. Spatial variability during other seasons is approximately 1°C. Relative to T_{min}, variability in T_{max} tends to be larger across models. Within each model simulation, seasonal variability in T_{min} and T_{max} are affected, in part, by the surface elevation of the grid cell.
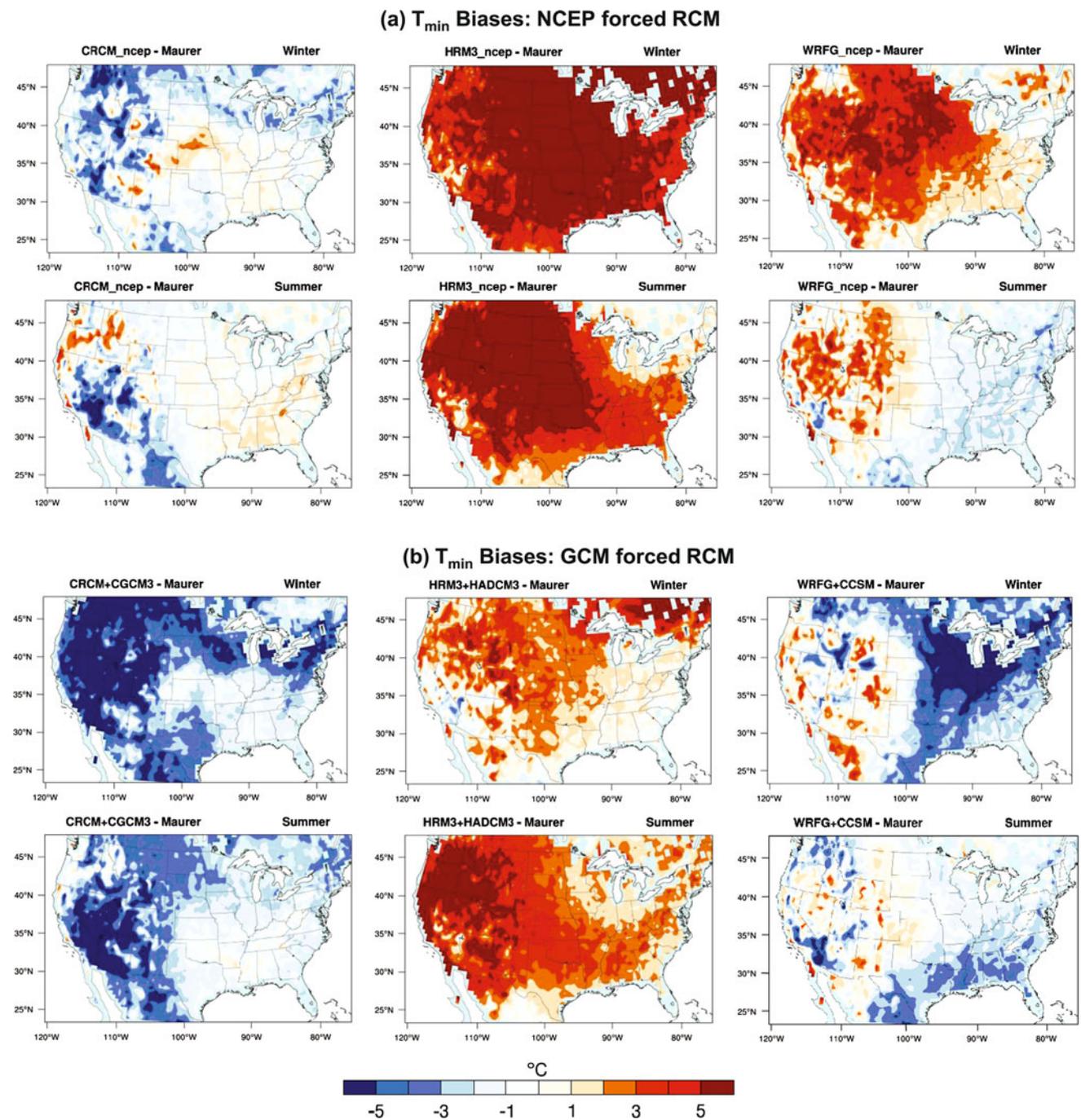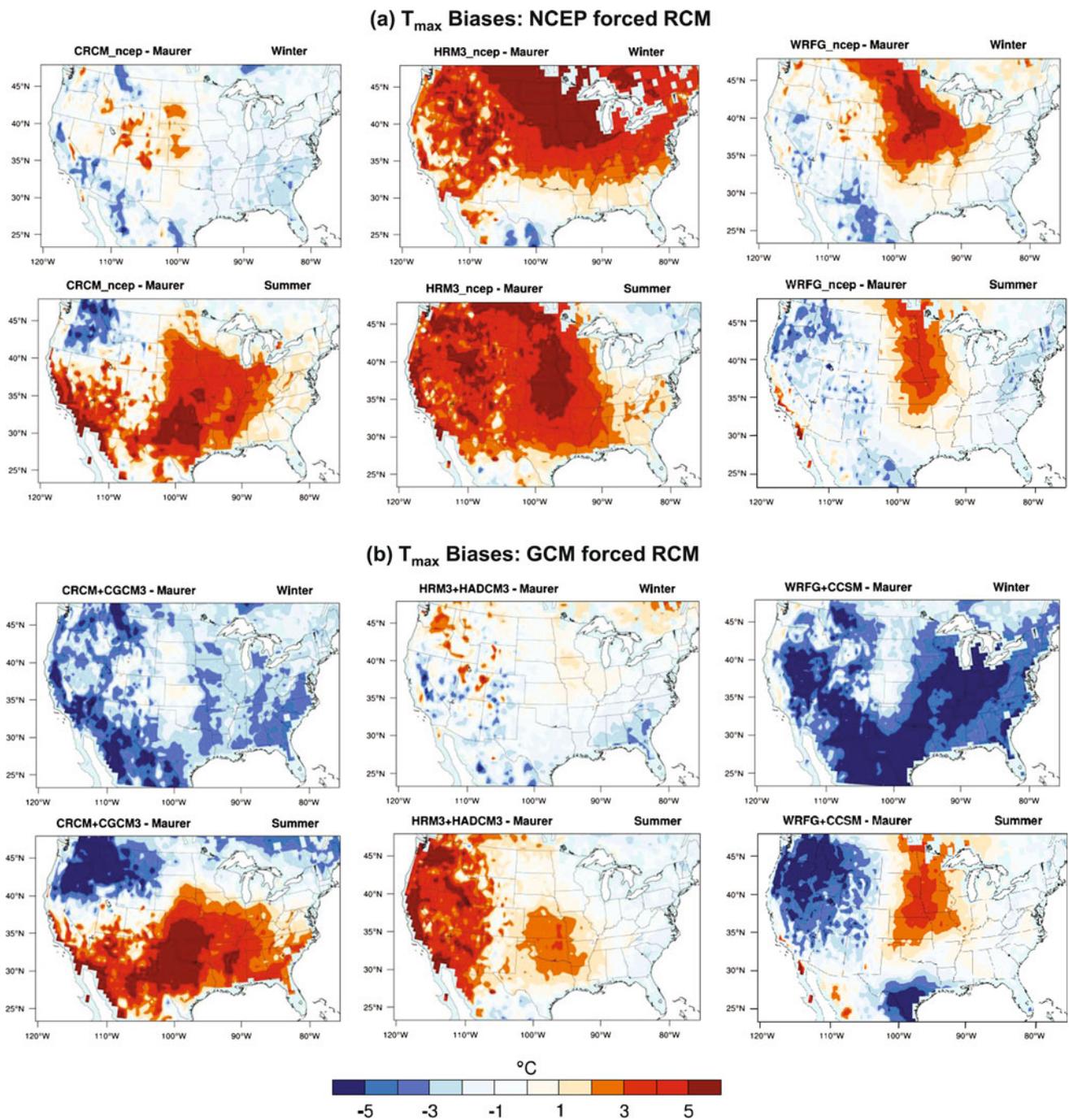
Fig. 2 Minimum temperature (T_{min}, °C) biases in the **a** NCEP and **b** GCM forced RCMs relative to the Maurer et al. (2002) gridded data for the conterminous US during winter (DJF) and summer (JJA). All datasets were interpolated to a standard half degree grid before calculating the bias. Time period considered for this computation is 1981–1999

Analysis of changes in T_{min} and T_{max} based on surface elevation is shown is Fig. 5. Results are presented for two elevation bands: 5,000–8,000 ft (1,500–2,450 m) and 8,000–11,000 ft (2,450–3,350 m). In general, there is a greater increase in winter T_{min} at lower elevations and in summer T_{max} at higher elevations. For winter, T_{min} experiences greater increases at lower elevations in the three model

simulations, which also produce large wintertime increases in T_{min} relative to other seasons. RCMs also show greater increases in T_{min} at lower elevations in all other seasons except for WRFG+CCSM, which have greater increases at higher elevations. For T_{max}, two simulations (HRM3+HADCM3 and WRFG+CCSM) show greater increases at lower elevation in winter. During spring, there are large

(a) T$_{max}$ Biases: NCEP forced RCM

(b) T$_{max}$ Biases: GCM forced RCM

Fig. 3 Maximum temperature (T$_{max}$, °C) biases in the **a** NCEP and **b** GCM forced RCMs relative to the Maurer et al. (2002) gridded data for the conterminous US during winter (DJF) and summer (JJA). All datasets were interpolated to a standard half degree grid before calculating the bias. Time period considered for this computation is 1981–1999

increases in T$_{max}$ at lower elevations—CRCM+CGCM3 and RCM3+CGCM3 simulate 0.5–1°C more daytime warming at the lower elevations. Conversely, summer and fall have greater increases in T$_{max}$ at higher elevations. Summer in particular experiences greater T$_{max}$ increases at higher elevations with more prominent responses simulated by CRCM+CGCM3 and HRM3+HADCM3.

3.2 Projected changes in surface energy balance

To explore the mechanism for increases in T$_{min}$ and T$_{max}$, we analyze changes in the surface energy fluxes between the 1971–2000 and 2041–2070 periods. Owing to data availability, this analysis is based only on two RCMs—CRCM+CGCM3 and HRM3+HADCM3. Figure 6 shows

Table 2 Seasonal correlation between reanalysis (North American regional reanalysis, NARR) and the three RCM (CRCM, WRFG, HRM3) anomalies in T_{min} and T_{max} for the study region for the 1979–2004 period

	T_{min}				T_{max}			
	NARR	CRCM	WRFG	HRM3	NARR	CRCM	WRFG	HRM3
Winter								
NARR	1.00	0.61	0.69	0.57	1.00	0.84	0.78	0.73
CRCM	–	1.00	0.67	0.57	–	1.00	0.84	0.78
WRFG	–	–	1.00	0.78	–	–	1.00	0.89
HRM3	–	–	–	1.00	–	–	–	1.00
Spring								
NARR	1.00	0.74	0.54	0.62	1.00	0.87	0.61	0.49
CRCM	–	1.00	0.57	**0.35**	–	1.00	0.68	0.71
WRFG	–	–	1.00	0.63	–	–	1.00	0.61
HRM3	–	–	–	1.00	–	–	–	1.00
Summer								
NARR	1.00	0.41	0.55	0.63	1.00	0.74	0.50	0.48
CRCM	–	1.00	0.57	**0.31**	–	1.00	0.65	0.42
WRFG	–	–	1.00	0.75	–	–	1.00	0.67
HRM3	–	–	–	1.00	–	–	–	1.00
Fall								
NARR	1.00	0.72	0.61	0.71	1.00	0.83	0.76	0.72
CRCM	–	1.00	0.68	0.76	–	1.00	0.80	0.60
WRFG	–	–	1.00	0.77	–	–	1.00	0.77
HRM3	–	–	–	1.00	–	–	–	1.00

The spatial scales involved in simulations are comparable for both NARR and the three RCMs. The bold values are not significant at the 0.05 level

mean seasonal anomalies in different components of the surface energy fluxes from the two RCMs. The analysis shows that, by mid-21st century, RCMs project large increases in both ULR (10–23 Wm^{-2}) and DLR (10–18 Wm^{-2}) with largest (smallest) increases in summer (winter) because of the modulation of surface longwave emission by surface temperature. However, there is a greater increase in the DLR-to-ULR ratio during winter relative to spring and summer.

RCMs also project large increases in ASR (6 W m^{-2}) during spring with smaller increases in winter and summer at lower and higher elevations, respectively. More strikingly, RCMs simulate large decreases in LAT (10 W m^{-2}) accompanied by similarly large increases in SEN (8 W m^{-2}) in summer. This pattern in LAT and SEN is also seen during fall for both simulations and during spring for HRM3+HADCM3, although these changes are much lower in magnitude than during the summer.

4 Seasonal warming: examining physical mechanisms

All the four RCM simulations considered in this study show 2°C or higher increases in T_{min} and T_{max} for all seasons. Although all seasons are showing a warming in excess of 2°C in the two temperature extremes, certain seasons are showing even larger changes in these parameters. Specifically, summer has that largest increases in the daytime maxima (3–4°C), and for winter, several models show similarly large increases in the nighttime minima. We hypothesize that the differences between small and large warming are due to changes in the relative strength of certain feedbacks and forcings. We examine both the interannual variability of T_{min} and T_{max} with other climate variables and the mean change between the future and past period in these climate variables to evaluate the strength of the relationships between temperature and other climate parameters.

To explore the mechanisms for the projected seasonal warming, we evaluate the simulated changes in the surface energy fluxes. Table 3 summarizes the important surface energy flux anomalies that contribute to increases in T_{min} and T_{max} during a particular season. Table 4 shows seasonal correlations of T_{min} and T_{max} with the different surface energy fluxes, precipitation, soil moisture, surface reflectivity, cloud cover and specific humidity between 2041 and 2070, and Table 5 shows the percent change in these variables between the 1971-2000 and 2041-2070

Fig. 4 Seasonal anomalies (°C) in (a) T_{min} and (b) T_{max} between 1971–2000 and 2041–2070 for the study region from four regional model simulations. *Contour lines* show elevation in feet
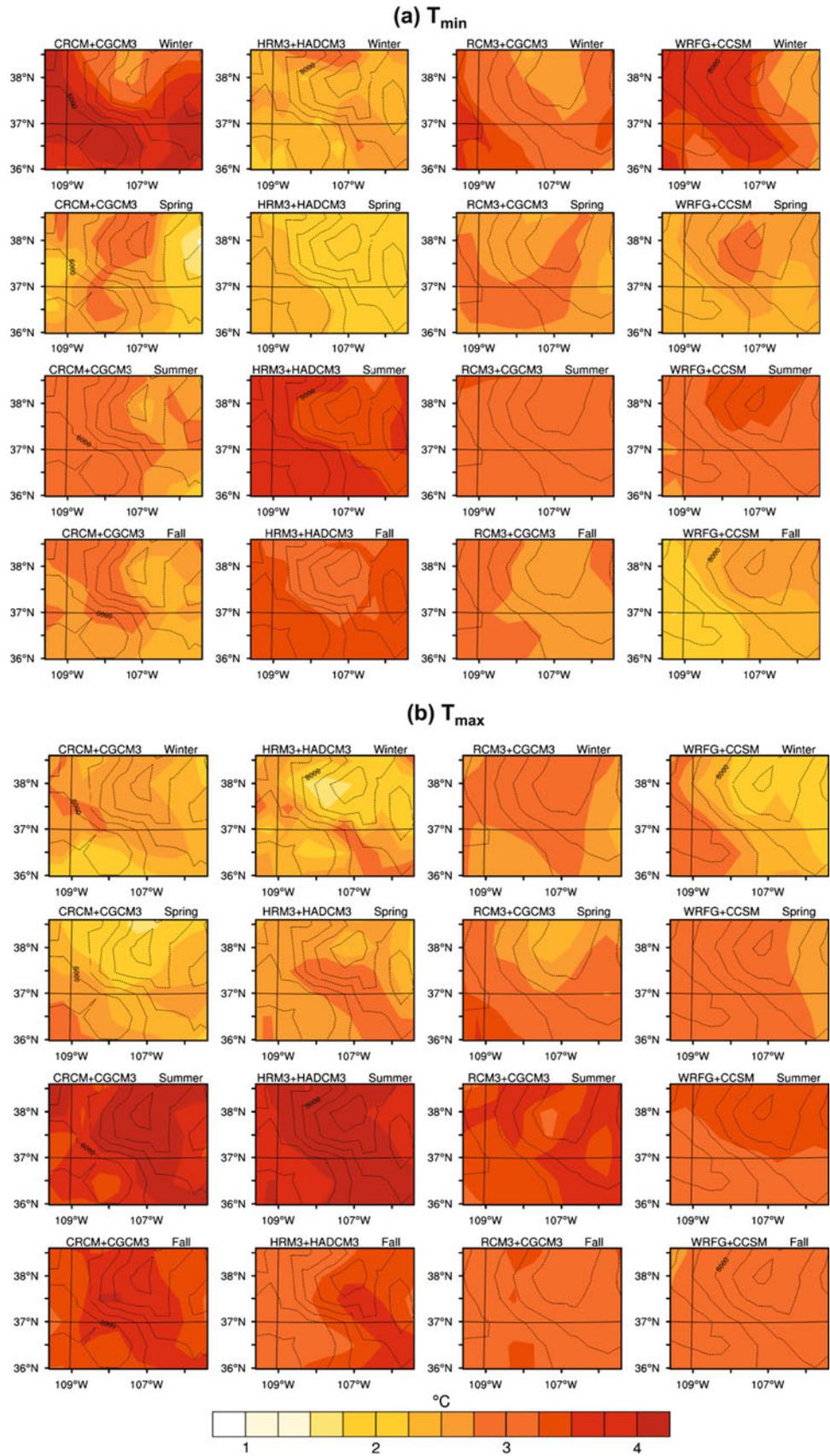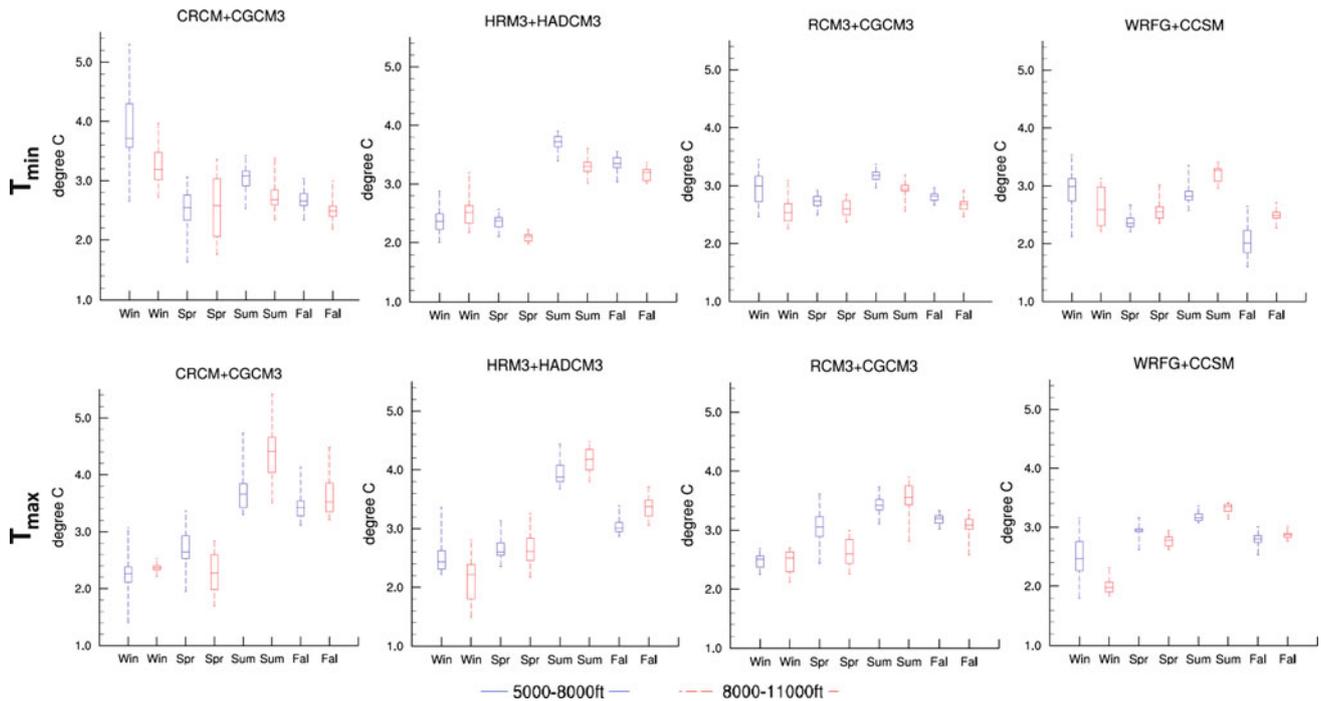
Fig. 5 Seasonal anomalies (°C) in T_{min} and T_{max} between 1971–2000 and 2041–2070 for the study region from four regional model simulations for two different elevation zones—5,000–8,000 ft and 8,000–11,000 ft. *Boxplots* describe the spatial variability. The boxes describe 25th and the 75th percentile values, the *dark line* is the median value and the *error bars* show the minimum and the maximum value

periods. We discuss these results separately for each season next with a much greater emphasis on winter and summer.

4.1 Winter

For winter, there are large increases in T_{min} at lower elevations in majority of the model simulations. It appears that increases in ASR, soil moisture and specific humidity, accompanied by proportionately higher increases in DLR relative to ULR, particularly at lower elevations, are largely responsible for these large increases in T_{min}.

Higher increases in DLR relative to ULR suggest the possibility of increases in atmospheric emissivity assuming that the land and the near-surface atmosphere have warmed up by the same amount. DLR increases occur because of the increases in ULR caused by surface warming. Most of this increase in ULR is absorbed, primarily, by clouds and water vapor in the atmosphere and reemitted to the surface as DLR. Both models show a strong modulation of DLR by cloud cover and specific humidity (Fig. 7). However, we find that increases in specific humidity explains most of the increases in DLR. Specific humidity, which increases by 15–25% by 2041–2070 in comparison to very little change in cloud cover (Table 5), explains greater interannual variability in DLR (see Fig. 7). Table 4 shows a high correlation (0.9) between specific humidity and T_{min}

between 2041 and 2070. Only one of the two models (HRM3+HADCM3) in Table 4 show a correlation (0.52) between cloud cover and T_{min}, although there is a small decrease in the mean cloud cover in that model between 2041 and 2070 relative to the 1971–2000 period (Table 5).

Increases in specific humidity have been suggested to cause proportionately greater increases in DLR during winter in high elevation regions (Ruckstuhl et al. 2007; Rangwala et al. 2010). At high altitude regions, particularly in the extratropics, the lower atmosphere tends to be optically under-saturated in water vapor absorption lines for longwave radiation, specifically during the cold season. Therefore, increases in water vapor during winter, when the specific humidity is lowest, would cause a large increase in DLR (Rangwala et al. 2010). These increases in DLR will primarily increase the minimum temperature. This process might, in part, be responsible for higher warming rates found during winter in the upland areas, globally, in both the observations (e.g., Liu and Chen 2000; Jungo and Beniston 2001; Pederson et al. 2010; Holden and Rose 2011) and climate models (e.g., Giorgi et al. 1997; Rangwala et al. 2010).

We use Ruckstuhl et al. (2007) observed relationship between DLR and specific humidity (q) from the Swiss Alps for cloud-free conditions (DLR = $150.4 \times q^{0.35}$) to estimate increases in DLR based on the RCMs' increases in
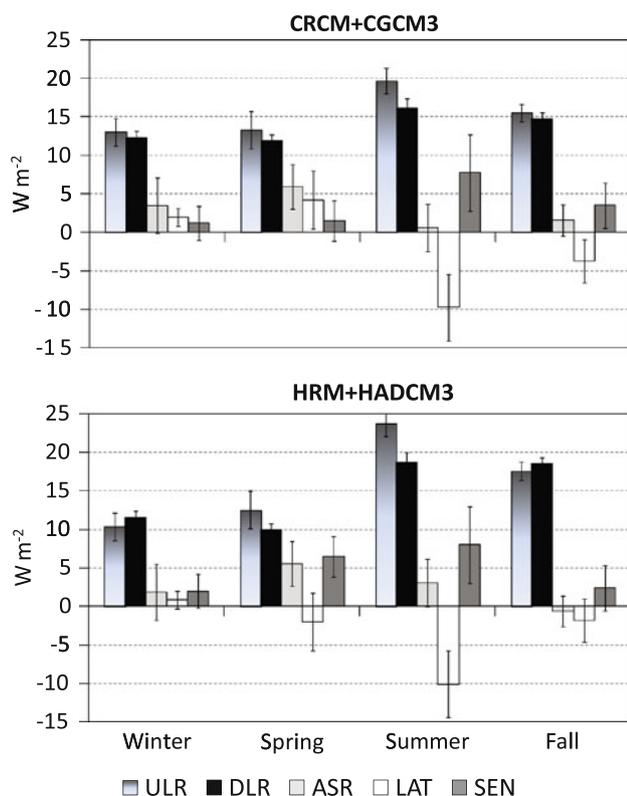
Fig. 6 Seasonal changes in surface energy fluxes (W m^{-2}) between 1971–2000 and 2041–2070 for the study region from two RCMs. The energy flux components include: Upwelling longwave radiation (ULR), downwelling longwave radiation (DLR), absorbed solar radiation (ASR), latent (LAT) and sensible (SEN) Heat

q. We obtain 10–16 W m^{-2} (5-6%) increase in DLR for 0.39–0.54 g/kg (14–25%) increase in q by 2041–2070, from HRM3+HADCM3 and CRCM+CGCM3 simulations, respectively. These estimated increases in DLR are comparable to the increases simulated by the two RCMs (Fig. 6), thus supporting our hypothesis. We calculated spatial correlation between the model changes in DLR by mid-21st century and the changes in DLR estimated from model changes in q using the relationship from Ruckstuhl et al. (2007) using output from CRCM+CGCM3 for the contiguous United States. We found a correlation coefficient of greater than 0.6 for all seasons but highest correlation was obtained for winter (r = 0.88), suggesting a stronger modulation of DLR by q in winter.

In CRCM+CGCM3, specific humidity increases by 10–50% across the contiguous United States in all seasons by mid-21st century. However, these percent increases are greater during winter and the higher values are generally found at higher latitudes. Some of these high increases occur in regions that also experience a greater loss in snow. The lower elevation region of our study area is one such example. It appears that the melting of snow in winter, in the model, in some regions is adding to the atmospheric moistening at the local scale. We find a much higher spatial correlation (r = 0.97 for the contiguous United States) during winter for percent changes, by mid-century, in DLR and q than for summer (r = 0.75). This further suggests that wintertime increases in q causes greater increases in DLR in the model.

The increase in ASR during winter is greater than the increase in the net downward longwave radiation. Therefore, we might expect similar or greater increases in T_{max} relative to T_{min} because the excess absorption of insolation by a greater proportion of snow-free surface should rapidly produce a more enhanced warming during the day. However, the model simulations do not show very large increases in T_{max} as they do for T_{min}. We hypothesize that the projected increases in winter snowmelt, particularly at lower elevations, and the concomitant increases in soil moisture counters the increases in ASR with increases in evapotranspiration and sublimation (LAT) processes. The increases in evapotranspiration during the day requires less sensible heat flux to satisfy the surface energy balance, thereby moderating the increase in T_{max}.

To better understand the changes in surface energy fluxes over the diurnal period, we separately analyze changes in surface energy fluxes for day and night from one RCM (CRCM+CGCM3) as shown in Fig. 8. During the day, there is a large increase in ASR (10 W m^{-2}). We also find greater increases in LAT during the day relative to the nighttime increases. There is a small decrease in SEN during the day, however SEN increases during the night and causes additional increases in the surface air temperature. At night, the DLR increases by 12.3 W m^{-2}. If the DLR were balanced entirely by an increase in ULR, then the change in surface temperature can be estimated using the relationship, $\Delta B/B = 4*\Delta T/T$, derived from the Stefan-Boltzmann law for black body radiation, where ΔB and ΔT

Table 3 Projected large seasonal day or nighttime warming and the associated changes in surface energy fluxes

Season	Daytime/nighttime warming	Important surface energy fluxes
Winter	Large nighttime warming (3–4°C)	Increases in DLR and ASR
Spring	Similar day & nighttime warming (2–3°C)	Large increases in ASR
Summer	Large daytime warming (3–4°C)	Large decreases in LAT and similar increases in SEN
Fall	Similar day & nighttime warming (2–3°C)	Decreases in LAT and increases in SEN

Table 4 Seasonal correlation (r) of Tmin and Tmax with precipitation, soil moisture, surface reflectivity, cloud cover, specific humidity and the components of surface energy fluxes from two RCM simulations

|	T_{min}				T_{max}			
	Winter	Spring	Summer	Fall	Winter	Spring	Summer	Fall
HRM3+HADCM3								
DLR	**0.91**	**0.75**	**0.63**	**0.77**	**0.43**	0.19	0.12	0.25
ASR	−0.22	0.05	0.18	0.20	**0.45**	**0.63**	**0.64**	**0.73**
LAT	0.31	0.05	−0.33	−0.12	−0.19	**−0.52**	**−0.74**	**−0.61**
SEN	−0.68	0.12	0.29	0.23	−0.33	**0.65**	**0.70**	**0.67**
Precipitation	0.30	0.01	−0.36	−0.11	**−0.29**	**−0.58**	**−0.77**	**−0.62**
Soil moisture	**0.39**	−0.18	−0.25	−0.18	−0.06	**−0.62**	**−0.47**	**−0.59**
Surf. reflectivity	**−0.58**	**−0.77**	−0.11	**−0.63**	**−0.83**	**−0.73**	−0.15	**−0.72**
Cloud cover	**0.52**	0.16	0.19	−0.12	−0.09	**−0.37**	−0.23	**−0.54**
Sp. humidity	**0.90**	**0.42**	−0.03	0.30	**−0.83**	**−0.73**	−0.15	**−0.72**
CRCM+CGCM3								
DLR	**0.64**	**0.78**	**0.83**	**0.85**	**0.47**	0.29	0.10	0.21
ASR	0.32	0.30	**−0.38**	0.12	**0.47**	**0.78**	**0.40**	**0.78**
LAT	**0.54**	0.36	−0.13	−0.08	**0.36**	−0.12	**−0.75**	**−0.71**
SEN	−0.03	0.05	−0.06	−0.04	0.01	**0.59**	**0.66**	**0.61**
Precipitation	−0.10	0.07	0.20	−0.07	−0.27	**−0.49**	**−0.57**	**−0.59**
Soil moisture	−0.12	**−0.38**	−0.31	0.08	−0.15	**−0.70**	**−0.54**	**−0.52**
Surf. reflectivity	**−0.59**	**−0.80**	**−0.52**	**−0.58**	**−0.52**	**−0.84**	0.22	**−0.54**
Cloud cover	−0.02	−0.04	0.27	0.05	−0.32	**−0.59**	−0.34	**−0.66**
Sp. humidity	**0.89**	**0.93**	**0.83**	**0.71**	**−0.52**	**−0.84**	0.22	**−0.54**

Bold values are significant at 5% level

Table 5 Mean percent changes by mid-21st century in precipitation, soil moisture, surface reflectivity, cloud cover, specific humidity and the components of surface energy fluxes from two RCM simulations

	HRM3+HADCM3				CRCM+CGCM3			
	Winter	Spring	Summer	Fall	Winter	Spring	Summer	Fall
DLR	5	4	6	7	6	5	6	6
ASR	2	3	1	0	4	3	0	1
LAT	5	−5	−18	−6	36	13	−23	−18
SEN	−10	20	16	10	9	4	11	10
Precipitation	4	−11	−20	0	4	−7	−25	−9
Soil moisture	2	0	−1	0	4	0	−3	−2
Surf. reflectivity	−10	−4	0	−3	−10	−11	0	−4
Cloud cover	−3	−3	−6	5	0	−5	3	−3
Sp. humidity	14	7	4	18	25	18	14	17

are changes in DLR and temperature, respectively. However, as stated above, the ratio of DLR to ULR increases in the winter in these model simulations so this simple calculation should somewhat overestimate the surface warming. This calculation yields $\Delta T = 4.1°C$ when $\Delta B = 12.3$ W m^{-2}, which is slightly larger than the mean simulated change in T_{min} of 3.7°C. By mid-century, the RCMs proj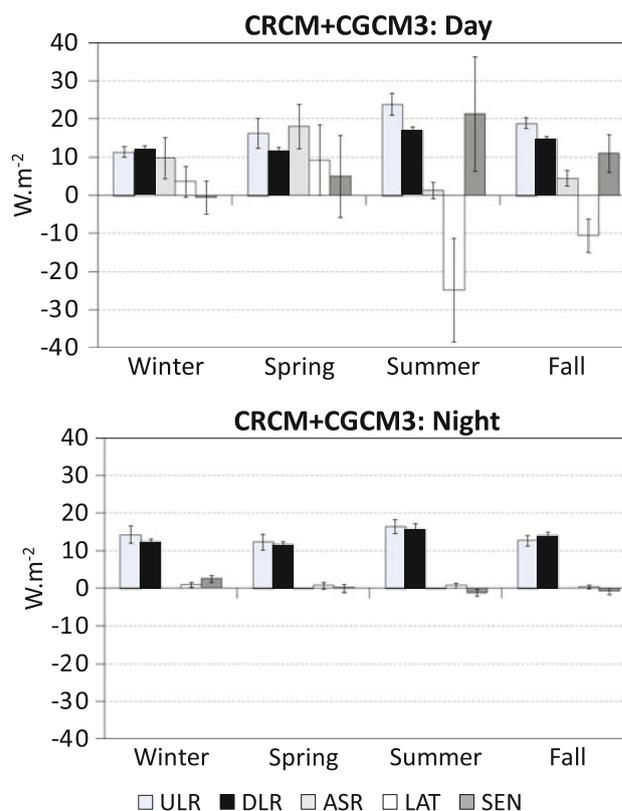ect increases in soil moisture and specific humidity during winter, particularly at lower elevations, due in part to increases in precipitation and snowmelt. The excess moisture in soil and atmosphere oppose the cooling mechanisms during the night because of its high specific heat capacity and the ability to absorb the increases in outgoing longwave emission from the surface, thereby causing larger increases in T_{min}. Therefore, we propose a "snow-albedo and moisture" feedback process during
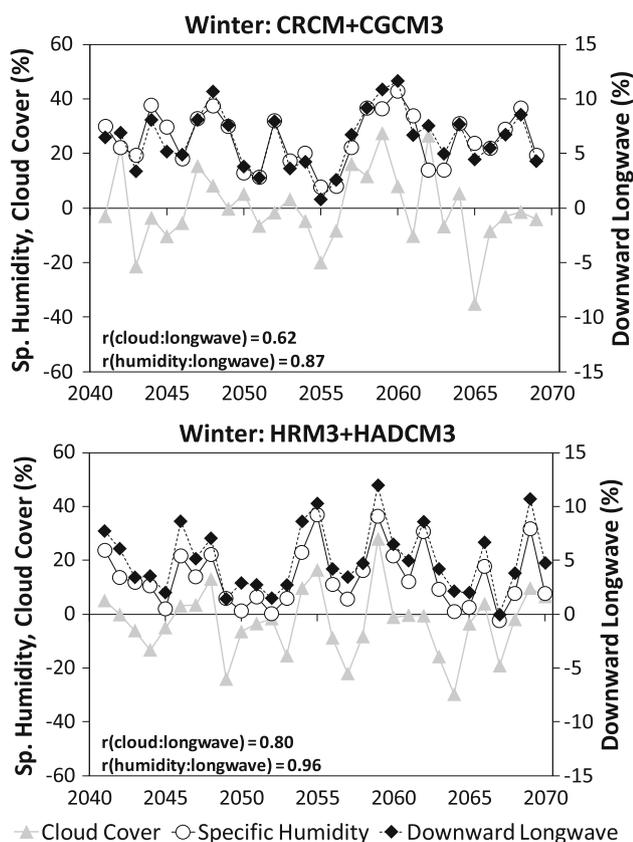
Fig. 7 Winter anomalies (%) in cloud cover, surface specific humidity (*left*) and downward longwave radiation (*right*) for the study region between 2041 and 2070 relative to the 1971–2000 mean from two RCMs

Fig. 8 Same as Fig. 6, but separately done for *day* and *night* for CRCM+CGCM3

winter where increases in the soil and atmospheric moisture in the model retain the daytime surface energy flux—primarily from increased absorption of incoming solar radiation owing to decreases in surface albedo—in the land–atmosphere system throughout the diurnal period such that the largest warming occurs in the nighttime temperatures.

It is interesting to note that HRM3+HADCM3 is the only RCM that does not simulate a large increase in winter T_{min} relative to other seasons. We find that there is a reduced snow covered surface during winter in the historical (1971–2000) climatology in HRM3+HADCM3 when compared to CRCM+CGCM3, particularly at the lower elevations. This might be due, in part, to the warm bias inherent in HRM3 (Fig. 2a) which is also apparent in the historical projection from HRM3+HADCM3 (Fig. 2b) but only at the higher elevations. However, the cold bias in CRCM at lower elevations in our study region (Fig. 2a) becomes much more pronounced in CRCM+CGCM3 historical simulation and extends over the whole study region (Fig. 2b). This may cause a greater historical snow coverage in the CRCM+CGCM3 and result in a simulation

of greater reductions in the wintertime snow covered surface at lower elevations by mid-century because of the atmospheric warming. These reductions in snow cover are commensurate with proportionate reduction in surface reflectivity (Figure S2 in Supplementary Material). Smaller reductions in winter snow cover, and thus surface reflectivity, in HRM3+HADCM3 by mid-century could have a restrained warming response from the snow albedo feedback mechanism.

DLR is strongly sensitive to changes in cloud cover. Even small increases in cloud cover will cause large increases in DLR at night and hence T_{min}. However, the projected wintertime cloud fraction from the two RCMs show small decreases (-3%) to no change from the historical period (Table 5). Moreover, there is a moderate correlation (0.52) between T_{min} and cloud cover in the future period in HRM3 + HADCM3 but no correlation in CRCM+CGCM3. There is also no correlation between T_{max} and seasonal cloud cover in both RCMs. Therefore, changes in the cloud fraction in these two simulations are not large enough to explain the mean changes in DLR and ASR.

There are examples of 21st century RCM simulations that have projected relatively large warming during winter, usually at higher latitudes (e.g., Kjellström et al. 2007;

Kjellström et al. 2010). Winter-time warming in these RCMs has generally been attributed to a reduction in snow-covered ground and changes in cloud cover. Under more aggravated emission scenarios (e.g. SRES A2) the RCMs project substantial depletion in winter snow amounts at mid-latitudes (Giorgi et al. 2004). In addition, Viterbo et al. (1999) have suggested that erroneous simulations of soil moisture freezing in RCMs can cause surface warming during winter. The soil moisture could be frozen during winter, particularly at higher elevations. Frozen soil will be less susceptible to increases in evapotranspiration. Daytime heating expended in melting the frozen soil will also tend to curtail the increases in T_{max}.

4.2 Summer

For summer, the models are nearly unanimous in projecting large increases in T_{max} at higher elevations. The T_{max} increases in the study region appear to be primarily associated with large decreases in LAT and equally large increases in SEN; both of these surface fluxes are also highly correlated to the increases in T_{max} (Table 4). In CRCM+CGCM3 and HRM3+HADCM3, the reductions in LAT appear to be largely a consequence of decreases in summer precipitation. Decreases in soil moisture, in part, because of decreases in spring and summer precipitation also contribute to reductions in LAT at higher elevations. Drying of the land surface reduces evapotranspiration and increases sensible heat fluxes to balance surface energy fluxes and, therefore, cause warming of the land surface, particularly during the day.

Figure 9 shows contours of elevation along with the spatial distribution of changes in LAT by mid-21st century from CRCM+CGCM3 and HRM3+HADCM3 over the study region. The decreases in LAT are generally greater at higher elevations. We compute equivalent changes in the latent heat flux based on terms in the moisture budget that result from mean changes in precipitation and soil moisture by mid-21st century. These computed changes from the moisture budget contributions are compared to simulated changes in LAT in Fig. 9. This analysis suggests a large influence of decreases in precipitation on the mean reductions in LAT simulated for the region. During summer, we hypothesize that evapotranspiration is balanced, in large part, by precipitation through a fast hydrologic cycle at the land surface in the model. Therefore, changes in evapotranspiration are strongly sensitive to precipitation in these simulations.

One difficulty in diagnosing the role of soil moisture is that the RCM output in the NARCCAP archive only provides an integrated soil moisture value from all soil layers. Therefore, even though the decreases in the integrated soil moisture value is about 1%, we expect moisture decreases in the upper layer of the soil to be much greater because that layer will be more quickly affected by atmospheric warming, decreases in precipitation, and changes in surface insolation and wind. There are greater decreases in soil moisture at higher elevations, which are more strongly correlated to decreases in LAT and increases in SEN as compared to the lower elevation region.

The biases in the historical GCM-forced RCM simulations may affect the extremes in projected warming in the RCMs. For example, CRCM+CGCM3 and HRM3+HADCM3, which have warm T_{max} biases (Fig. 3), also project higher increases in T_{max}. On the other hand, WRFG+CCSM, which has a cold bias for our region, projects comparatively smaller increases in summer T_{max}. The biases in precipitation and T_{max} are closely related. RCM biases associated with excessive drying of soils and large reduction in surface latent heat fluxes in the present climate may contribute to large erroneous daytime warming in summer (Murphy 1999; Vidale et al. 2003; Moberg and Jones 2004; Anders and Rockel 2009).

Studies from other regional model projections, primarily from Europe, have generally found greatest changes in temperature extremes during summer (e.g., Hagemann et al. 2001, Rummukainen et al. 2001, Frei et al. 2003; Fischer et al. 2007; Kjellström et al. 2007; Kjellström et al. 2010). Rowell and Jones (2006) suggest two important mechanisms for large increases in summer daytime maxima over Europe: (1) summer-time warming in the lower troposphere leading to decreases in relative humidity over land, and (2) spring-time soil moisture reductions.

RCM responses are substantially modulated by the boundary conditions provided by the forcing GCM (e.g. Rummukainen et al. 2001; Giorgi et al. 2004) except during summer, when the responses of the RCM and GCM may diverge significantly (Giorgi et al. 2004). This is because regional physical processes (e.g., convection, soil moisture-precipitation feedbacks, etc.) are more dominant than large-scale atmospheric systems in summer over the mid-latitudes. There are also substantial increases in the interannual variability of both temperature and precipitation during summer whereas smaller changes occur during other seasons (Giorgi et al. 2004). The regional climate predictability in the RCMs is also found to be weakest during summer over the continental regions (Murphy 1999; Vidale et al. 2003).

Inter-RCM differences in model formulation can contribute significantly to the uncertainty in RCM responses during summer (Frei et al. 2006). For example, we find large differences in soil moisture climatologies between RCMs (Figure S3 in the Supplementary Material) which could arise from the difference in land surface schemes. In model formulation, the land surface scheme, cumulus parameterization and soil characterization play an
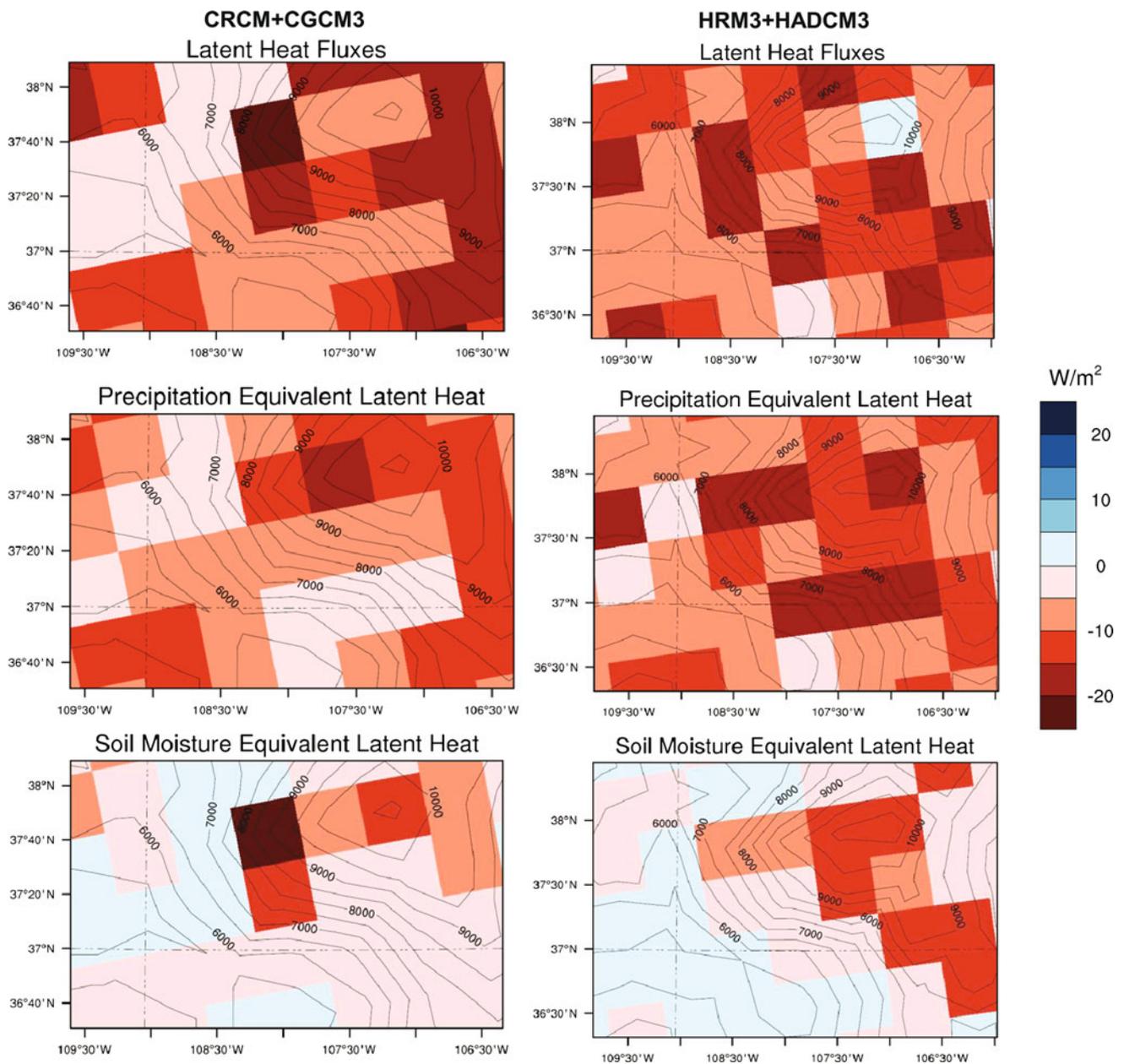
Fig. 9 Spatial representation of summer-time anomalies (W m^{-2}) in LAT (*top plots*) in the study region between the 2041–2070 and 1971–2000 periods from CRCM+CGCM3 and HRM3+HADCM3. The changes in LAT are compared to equivalent latent heat of vaporization associated with changes in moisture balance as a result of changes in precipitation (*middle plots*) and soil moisture (*bottom plots*). *Contour lines* show elevation in feet

exceedingly important role during summer (e.g. Hagemann et al. 2001; Vidale et al. 2003; Moberg and Jones 2004). Because these processes are coupled, it is quite challenging to attribute the RCM biases in temperature and soil moisture to specific inter-model differences. Considering the large decreases (−20%) in projected summer precipitation from most of the RCMs (Figure S4 in the Supplementary Material) and its influence on decision-making by land and water managers, it is crucial to reduce uncertainties associated with these parameterizations.

4.3 Spring and fall

For spring, the magnitude of increases in T_{min} and T_{max} are similar. The projected warming is largely associated with increases in ASR (<5%), which occurs, primarily, because of the reduction in the snow and cloud cover. We use changes in surface reflectivity, which is a ratio of the incoming to outgoing solar radiation, as a proxy for changes in snow cover. Both model simulations project decreases in the snow (−5 to −10%) and cloud cover
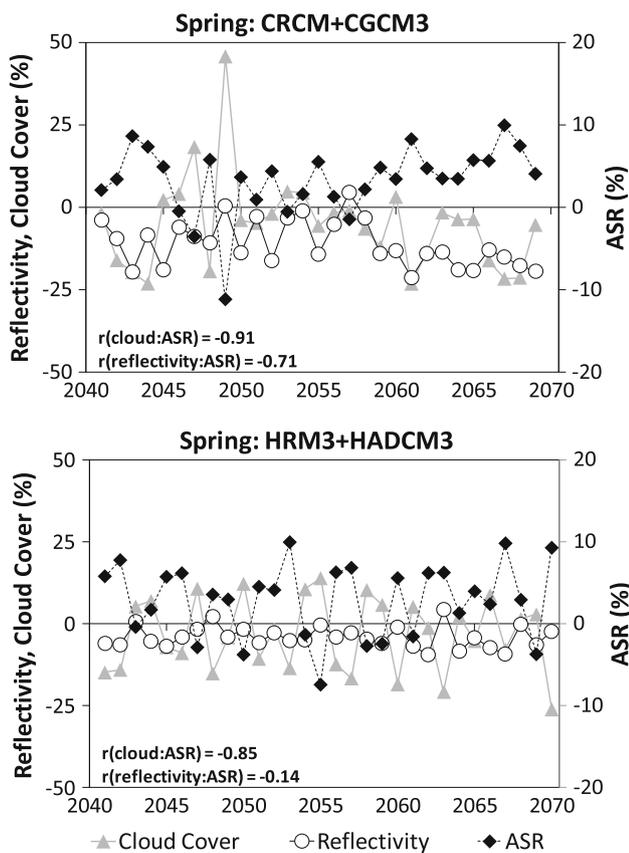
Fig. 10 Spring anomalies (%) in cloud cover, surface reflectivity (*left*) and absorbed solar radiation at surface (ASR, *right*) for the study region between 2041 and 2070 relative to the 1971–2000 mean from two RCMs

(−5%). However, cloud cover explains greater interannual variability in ASR (Fig. 10; r = −0.85 to −0.91). Correlation between snow cover and ASR varies greatly between the two models; HRM3+HADCM3 shows very little negative correlation between the two. Relative of higher elevations, there are greater decreases in soil moisture during spring at lower elevations.

For fall, RCMs project greater increases in T_{max} relative to T_{min}; a pattern which is similar to summer although the magnitude of the change during fall is smaller. The pattern of decreases in LAT and increases in SEN and their relationship with moisture availability found in summer is also true during fall. However, the magnitude of changes in LAT and SEN are also smaller. Snow cover decreases are smaller in fall relative to winter and spring, which also account, in part, for smaller increases in ASR.

5 Conclusions

This study analyzed projections in T_{min} and T_{max} by mid-21st century from four RCMs, driven by three different

GCMs, for the San Juan Mountains and the Four Corners Region which are part of the Rocky Mountain region in southwestern United States. We find that the different RCMs demonstrate consistency in simulating physical processes that lead to future changes in surface energy budgets and the associated warming response on seasonal and elevational scales despite their inherent biases. These processes include earlier snowmelt and thawing of soils as well as moistening of lower atmosphere in winter particularly at lower elevations; and, in summer, the RCMs simulate strong sensitivities for evapotranspiration to changes in precipitation and soil moisture. By mid-21st century, the RCMs simulate large changes in the long-term mean of energy and moisture budgets at the land surface relative to the historical period, on both seasonal and elevation bases, which are consistent with our physical understanding of these processes.

Regarding temperature extremes, the RCMs project a warming in excess of 2°C in both T_{min} and T_{max} for all seasons. However, there are much greater increases (3–4°C) in T_{min} during winter and T_{max} during summer. The normal daytime summer temperatures by 2050 are projected to be similar to those observed in 2002, which are some of the highest recorded summer temperatures in the region (Rangwala and Miller 2011).

Figure 11 provides a conceptual framework of the changes in physical factors that are associated with large increases in winter T_{min} and summer T_{max}. The T_{min} increases in winter are, in part, associated with decreases in surface snow cover and increases in soil moisture and specific humidity. Reductions in snow covered surface causes increases in the absorption of daytime insolation by the land surface. However, the increased moistening of the soil and atmosphere facilitates a greater diurnal retention of the daytime solar energy in the land surface and amplifies the longwave heating of the land surface at night. The summer-time increases in T_{max} are associated with large decreases in latent heat fluxes caused, in large part, by the moisture deficit at the land surface from decreases in precipitation. The decreases is soil moisture during summer, particularly at higher elevations, further contribute to the increases in T_{max}.

Surface energy flux measurements by Turnipseed et al. (2002) at a site in the Colorado Rocky Mountains, during the years of 1999 and 2000, support some of the basic physical explanation that we have proposed for seasonal changes in the surface energy fluxes by mid-21st century that drive the changes in T_{min} and T_{max}. They found that sensible heat fluxes dominate the time period prior to the snowmelt season in part because soils are frozen even though air temperatures are warm enough for transpiration. However, as soon as liquid water is available from snowmelt, the latent heat fluxes become equal or greater than
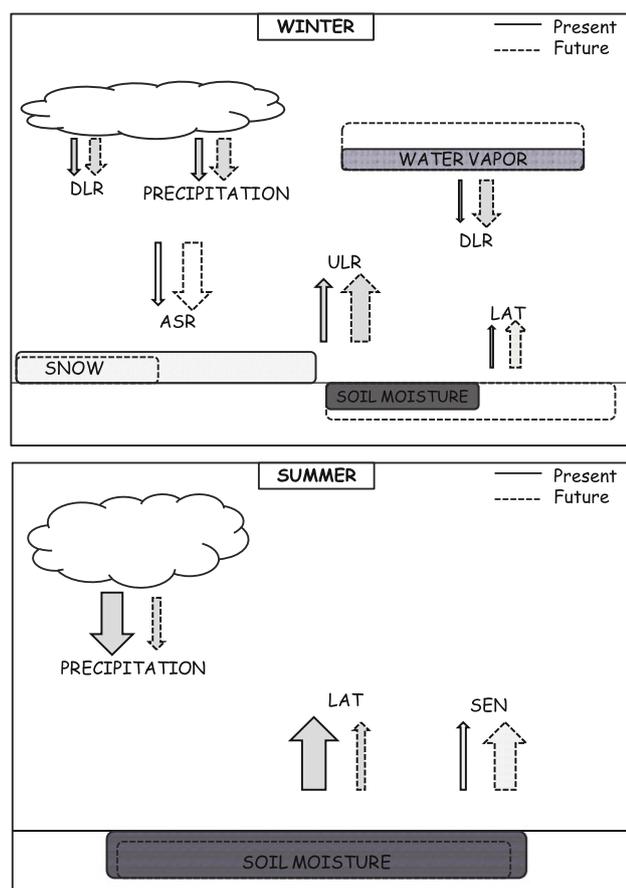
Fig. 11 Conceptual framework of important changes by mid-21st century in surface energy fluxes and moisture balance simulated by the regional models for winter (*above*) and summer (*below*)

sensible heat fluxes. This is consistent with our hypothesis here that low elevation regions in these RCMs experiments have a greater amount of liquid water available in winter, partly because of early snowmelt, which results in increases in the daytime latent heat fluxes by mid-21st century. For summer, they found that daytime latent heat fluxes are tied to the frequency of rain and soil moisture. Between late-July and mid-August of 2000, when monsoonal flow was cut-off from Colorado, there were significant decreases in daytime latent heat fluxes relative to the same time period in 1999 when the site was not water stressed.

Part of the large summer-time increases in T_{max} could be the result of deficiencies in model formulations of sub-grid scale processes—particularly those associated with the land-surface scheme (that may cause excessive soil drying) and the convective parameterization scheme (that may affect convective precipitation). Additional uncertainties arise from future changes in precipitation associated with changes in storm tracks and the simulation of the North American summer monsoon. Realistic projections in summer precipitation are dependent on adequate representation of monsoonal flows into this region. A

preliminary analysis suggests that the monsoonal precipitation pattern remains challenging to simulate in these RCMs. Accordingly, the summertime T_{max} projections here may be less reliable than other seasonal temperature changes. For our study region, we find that RCMs projections of wintertime increases (5–10%) and summer-time decreases (−10 to −20%) in precipitation are closer to the central tendency of the CMIP3 models projections (Figure S5 in the Supplementary Material). Furthermore, it is difficult to assess how the RCM's biases in T_{min} and T_{max} affected the projected changes in these variables because the relationships are not straightforward. For example, we find that CRCM+CGCM3 has a large cold bias in winter (Figs. 2b, 3b) that may account for an increased snow cover area in our study region at lower elevations over the historical period relative to HRM3+HADCM3 which has a small warm bias. Future reduction in snow cover is found to be greater in CRCM+CGCM3, in part because of larger snow-covered surface in the baseline historical period, which leads to a relatively greater warming in this model caused by a stronger snow-albedo feedback mechanism. Therefore, in this example a colder bias in the historical simulation leads to greater warming in the future.

In comparison to the GCMs, the RCMs facilitate an improvement in the analysis of processes in mountainous regions because of the better resolution of the freezing level and elevation sensitive processes, including the modulation of DLR by water vapor. Despite these improvements in the orographic representation of physical processes, the NARCCAP RCMs are limited by their ∼50 km resolution and, therefore, only provide a weak mountain forcing for this region. From this analysis, it is difficult to infer future changes in T_{min} and T_{max} for elevations above 11,000 ft (3,350 m). A realistic mountain forcing that reproduces observed atmospheric cold-season dynamics at local scale can only be generated at model resolution of 6 km or less in these mountains (Rasmussen et al. 2011). A realistic orographic response will also significantly affect the seasonal snow to rain ratio as well as the seasonal snow cover, thereby affecting the surface energy balance and its impact on seasonal changes in T_{min} and T_{max}.

Despite the uncertainties extant in the RCMs, the observed warming pattern in recent decades (e.g. Rangwala and Miller 2010) is in accord with the seasonal warming projections from the RCMs. Particularly, the large increases in T_{max} at higher elevations in summer and similarly large increases in T_{min} at lower elevations in winter. RCMs projections are physically realistic in depicting wintertime decreases in snow cover and increases in soil moisture and humidity as well as summer-time decreases in soil moisture and evaporative fluxes. Notwithstanding a major shift in future precipitation relative to those projected in these

RCMs, we expect that these model results provide useful information for a physically based warming scenario by mid-21st century under business as usual emissions in the anthropogenic greenhouse gases.

References

Anders I, Rockel B (2009) The influence of prescribed soil type distribution on the representation of present climate in a regional climate model. Clim Dyn 33(2):177–186

Bonfils C et al (2008) Detection and attribution of temperature changes in the mountainous western United States. J Clim 21(23):6404–6424

Clow DW (2010) Changes in the timing of snowmelt and streamflow in Colorado: a response to recent warming. J Clim 23(9):2293–2306

Daly C et al (2008) Physiographically sensitive mapping of climatological temperature and precipitation across the conterminous United States. Int J Climatol 28(15):2031–2064

DOI (2009) Addressing the impacts of climate change on America's water, land, and other natural and cultural resources. United States Department of Interior. http://www.doi.gov/archive/climatechange/SecOrder3289.pdf

Fischer E et al (2007) Contribution of land-atmosphere coupling to recent European summer heat waves. Geophys Res Lett 34(6):L06707

Frei C et al (2003) Daily precipitation statistics in regional climate models: evaluation and intercomparison for the European Alps. J Geophys Res 108(D3):4124

Frei C et al (2006) Future change of precipitation extremes in Europe: intercomparison of scenarios from regional climate models. J Geophys Res 111(D6):D06105

Giorgi F et al (1997) Elevation dependency of the surface climate change signal: a model study. J Clim 10:288–296

Giorgi F et al (2001) Regional climate information–evaluation and projections. In: Houghton JT et al (eds) Climate change 2001: the scientific basis. Cambridge University Press, pp 583–638

Giorgi F et al (2004) Mean, interannual variability and trends in a regional climate change experiment over Europe. II: climate change scenarios (2071–2100). Clim Dyn 23(7–8):839–858

Hagemann S et al (2001) The summer drying problem over southeastern Europe: sensitivity of the limited area model HIRHAM4 to improvements in physical parameterization and resolution, Physics and Chemistry of the Earth, Part B. Hydrol Ocean Atmosphere 26(5–6):391–396

Holden J, Rose R (2011) Temperature and surface lapse rate change: a study of the UK's longest upland instrumental record. Int J Climatol 31(6):907–919

Howe C et al (2011) Watershed vulnerability assessment pilot project: case study: Grand Mesa, Uncompahgre and Gunnison National Forests. Draft—April 4, 2011. ftp://ftp2.fs.fed.us/incoming/r2/gmug/WVA/WVA_GMUG_pilot_report04112011.pdf

Jungo P, Beniston M (2001) Changes in the anomalies of extreme temperature anomalies in the 20 th century at Swiss climatological stations located at different latitudes and altitudes. Theor Appl Climatol 69(1):1–12

Kjellström E, Giorgi F (2010) Introduction to the special issue on "Regional climate model evaluation and weighting". Clim Res 44:117–119

Kjellström E et al (2007) Modelling daily temperature extremes: recent climate and future changes over Europe. Clim Chang 81:249–265

Kjellström E et al (2010) 21st century changes in the European climate: uncertainties derived from an ensemble of regional climate model simulations. Tellus A 63(1):24–40

Liang X-Z et al (2008) Regional climate models downscaling analysis of general circulation models present climate biases propagation into future change projections. Geophys Res Lett 35(8):L08709

Liu X, Chen B (2000) Climatic warming in the Tibetan Plateau during recent decades. Int J Climatol 20(14):1729–1742

Maurer E et al (2002) A long-term hydrologically based dataset of land surface fluxes and states for the conterminous United States. J Clim 15(22):3237–3251

Mearns LO et al (2007) The North American Regional Climate Change Assessment Program dataset, National Center for Atmospheric Research Earth System Grid data portal, Boulder, CO. Data downloaded 2011-04-27. http://www.earthsystemgrid.org/browse/viewProject.htm?projectId=ff3949c8-2008-45c8-8e27-5834f54be50f (updated 2011)

Mearns L et al (2009) A regional climate change assessment program for North America. Eos Trans AGU 90(36):311

Moberg A, Jones PD (2004) Regional climate model simulations of daily maximum and minimum near-surface temperatures across Europe compared with observed station data 1961–1990. Clim Dyn 23(7):695–715

Murphy J (1999) An evaluation of statistical and dynamical techniques for downscaling local climate. J Clim 12(8):2256–2284

Pederson GT et al (2010) A century of climate and ecosystem change in Western Montana: what do temperature trends portend? Clim Chang 98(1):133–154

Rangwala I, Miller JR (2010) Twentieth century temperature trends in Colorado's San Juan Mountains. Arct Antarct Alp Res 42(1):89–97

Rangwala I, Miller JR (2011) Long-term Temperature Trends in the San Juan Mountains. In: Blair R, Bracksieck G (eds) EASTERN SAN JUAN MOUNTAINS: Their Geology, Ecology and Human History. University Press of Colorado, Boulder

Rangwala I et al (2010) Using a global climate model to evaluate the influences of water vapor, snow cover and atmospheric aerosol on warming in the Tibetan Plateau during the twenty-first century. Clim Dyn 34(6):859–872

Rasmussen R et al (2011) High-resolution coupled climate runoff simulations of seasonal snowfall over Colorado: a process study of current and warmer climate. Bull Am Meteorol Soc 24:3015–3048

Ray J et al (2008) Climate Change in Colorado. A synthesis to support water resources management and adaptation. A report for the Colorado Water Conservation Board., edited, Colorado Water Conservation Board, Denver. Western Water Assessment and University of Colorado, Boulder

Rowell DP, Jones RG (2006) Causes and uncertainty of future summer drying over Europe. Clim Dyn 27:281–299

Ruckstuhl C et al (2007) Observed relationship between surface specific humidity, integrated water vapor, and longwave downward radiation at different altitudes. J Geophys Res 112(D3):D03302

Rummukainen M et al (2001) A regional climate model for northern Europe: model description and results from the downscaling of two GCM control simulations. Clim Dyn 17(5):339–359

Salzmann N et al (2007) The application of regional climate model output for the simulation of high-mountain permafrost scenarios. Global Planet Chang 56(1–2):188–202

Turnipseed A et al (2002) Energy budget above a high-elevation subalpine forest in complex topography. Agric For Meteorol 110:177–201

USBR (2009) Colorado river basin water supply and demand study. United States Bureau of Reclamation. http://www.usbr.gov/lc/region/programs/crbstudy.html

USBR (2010) West-Wide climate risk assessments. United States Bureau of Reclamation. http://www.usbr.gov/WaterSMART/wwcra.htmlUSFS (2011) USDA forest service unveils proposed planning rule to provide science-based framework to support healthy forests and communities. United States Forest Service. http://www.fs.fed.us/r5/modoc/news/2011/Proposed%20Planning%20Rule%20Released_2_10_11.pdf

USFS (2011) USDA forest service unveils proposed planning rule to provide science-based framework to support healthy forests and communities. United States Department of Agriculture. USDA News Release No. 0061.11

Vidale PL et al (2003) Predictability and uncertainty in a regional climate model. J Geophys Res 108(D18):4586

Viterbo P et al (1999) The representation of soil moisture freezing and its impact on the stable boundary layer. Q J R Meteorol Soc 125(559):2401–2426